JCTC Journal of Chemical Theory and Computation

Computational Investigation of Wave Packet Scattering in the Complex Plane: Dynamics of Exact Quantum Trajectories

Robert E. Wyatt and Brad A. Rowland*

Department of Chemistry and Biochemistry, University of Texas, Austin, Texas 78712

Received June 26, 2008

Abstract: In two previous studies, the time-dependent scattering of a wave packet from a Gaussian barrier was investigated computationally in the complex *z*-plane. One of these involved the 'direct' propagation of the wave packet in the complex space, and the other used numerical analytic continuation techniques to generate the dynamics in the complex plane from the wave function computed on the real-axis. In the current study, the dynamics of exact quantum trajectories are analyzed for the same barrier scattering problem. Thousands of quantum trajectories were launched from positions near the center of the initial wave packet. These trajectories were computed by integrating equations-of-motion involving the quantum momentum function, which was obtained from the time-dependent wave function and its derivative. In order to analyze the dynamics, many trajectories were plotted on space-time diagrams. Particular emphasis was placed upon trajectories undergoing reflection in the barrier region. Some groups of strongly correlated trajectories form long-lived highly organized patterns, including helical wrappings around a series of stagnation filaments. These curves alternate with quasi-nodes where the amplitude of the wave function reaches low values. In addition, other trajectories for short times follow hyperbolic paths as they propagate near vorticity tubes surrounding these quasi-nodes.

1. Introduction

The current study is an extension of our previous investigations on wave packet scattering from a barrier potential in the complex plane.[1,2] This 'extended' 2D scattering problem was approached in two quite different ways: 'direct' propagation of a wave packet in the 2D complex *z*-space[1] and numerical continuation into the complex plane of time-dependent information computed on the real-axis.[2] The rich dynamics ensuing in the complex plane were analyzed by plotting the amplitude of the wave function and several other functions. In the introductory sections of these studies, we reviewed the use of complex-valued classical trajectories, analytical quantum trajectories computed for systems where the wave function is known, and for synthetic approximate quantum trajectories wherein information (namely, the quantum action function) is computed along each trajectory so that the wave function may be synthesized on-the-fly. Our previous papers should be consulted for references to these earlier studies.

The current study, dealing with 'exact' quantum trajectories for a nonstationary scattering problem, complements the detailed analysis of complex-valued quantum trajectories for one-dimensional *stationary state* scattering problems (the Eckart barrier, the soft potential step, and a downhill potential with a barrier).[3,4] The only previous studies of complex quantum trajectories for *nonstationary* problems have dealt with barrier-free systems for which the time-dependent wave function is known (or can be found) analytically; these include the free Gaussian wave packet[3] and the frontal collision of two Gaussian wave packets.[5]

In the current study, thousands of quantum trajectories were evolved in the complex space for the barrier scattering problem. In order to do this, the quantum momentum function along each trajectory was computed from the time-dependent wave function which was simultaneously computed on a large computational grid. Time histories of the

* Corresponding author e-mail: barowland@gmail.com.

10.1021/ct8002496 CCC: $40.75
Published on Web 01/29/2009

Table 1. Categories of Quantum Trajectories

type	description
transmitted	transmit beyond barrier maximum ($x > x_b$)
reflected trajectories:	
upper	propagate toward upper part of barrier region
down-up	move down initially and deflect toward larger value s of y without loops or spirals
loop-simple	move in toward barrier and deflect toward larger values of y without spirals
loop-down	move in toward barrier and deflect toward smaller values of y without spirals
loop-complex	move upward as propagation proceeds in toward barrier and reflect toward smaller values of y with some undulations
twist	move upward as propagation proceeds in toward barrier and then reflect toward smaller values of y with several loops or spirals
spiral	move upward as propagation proceeds in toward barrier and then reflect toward smaller values of y with complex spiraling

reflected trajectories were studied in detail, because many of them have much more complicated features than the transmitted trajectories. In addition, strong correlation between these trajectories leads to the formation of highly organized patterns. In space-time diagrams for the reflected wave packet, we will identify *vorticity tubes* (to be defined shortly). Groups of quantum trajectories coming from widely separated initial locations end up wrapping around stagnation curves which form in pairs adjacent to these tubes. Other quantum trajectories experience 'hyperbolic indentations' when they pass near the vorticity tubes. The helical coils of trajectories around the stagnation curves and the hyperbolic flow near vorticity tubes exemplify the most complicated types of trajectories that form during the reflection of the wave packet.

In an analysis of quantum vorticies that form around nodes in the complex plane for *stationary states*,[6] vector maps of the QMF were shown to exhibit hyperbolic flow close to these nodes. However, when the Pólya vector field,[7,8] defined as the conjugate of the QMF ($P(z) = p^*(z)$), is plotted, circular counterclockwise flow is obtained near the nodes. The vorticity, the curl of the Pólya field, $\vec{\Omega}(z) = \vec{\nabla} \times \vec{P}(z)$, provides a quantitative measure of the circulation of this field. For *nonstationary states*, as time proceeds, the nodes generally translate along curves, and this leads to time-dependence of the vorticity field. At a particular time, if a closed curve encloses a nodal region such that the magnitude of the vorticity is constant on this curve, then for later times a vorticity tube is formed by the isosurface surrounding this nodal curve. (As a historical note, Helmholtz introduced vorticity tubes[9] into hydrodynamics in 1858). For purposes of the current study, the vorticity tube will be defined as an

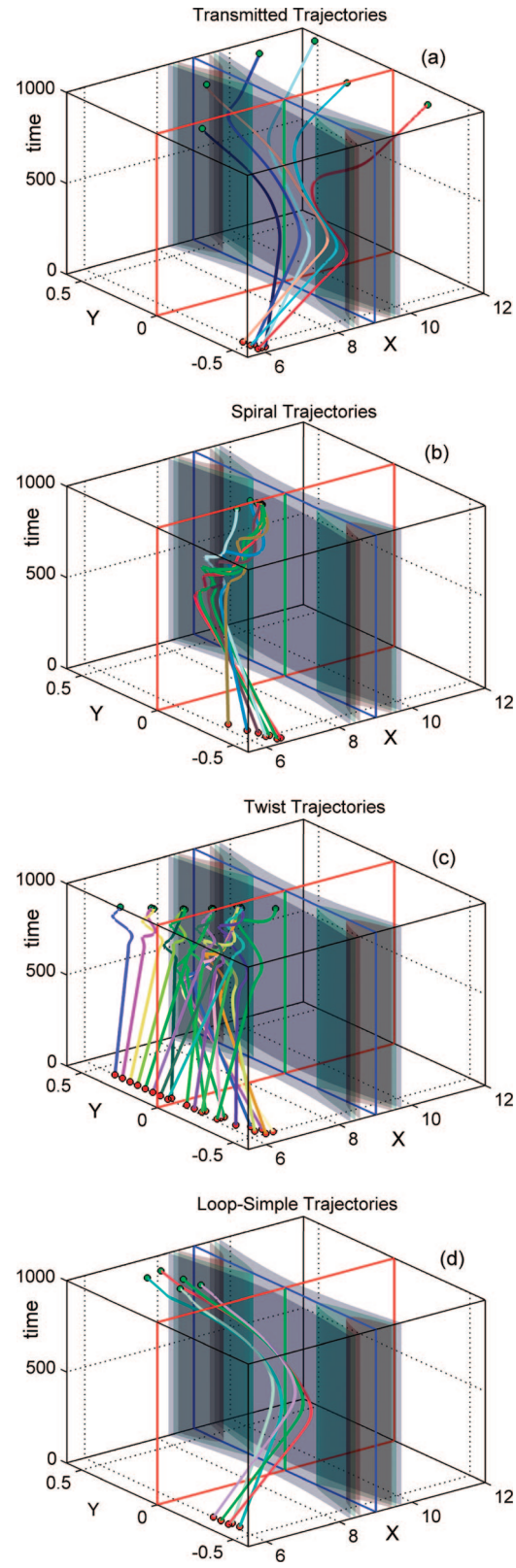

Figure 1. Time-dependence for four groups of quantum trajectories: (a) transmitted trajectories; (b) spiral trajectories; (c) twist trajectories; and (d) loop-simple trajectories. Propagation time is plotted on the vertical axis above the complex plane. In each part, the vertical slabs are isosurfaces of the absolute value of the potential energy.

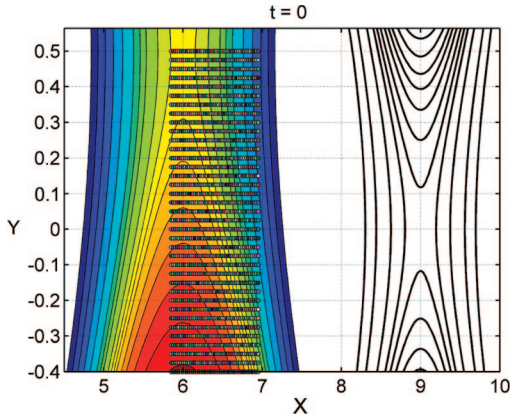

Figure 2. Contours (color) of log $_{10}|\psi|$ for the initial wave packet in the complex plane. Contours (black) of the magnitude of the potential, $|V(z)|$, are shown on the right side of the figure. In addition, a 45 × 43 grid of quantum trajectories at their initial locations are shown (colored dots).

isosurface corresponding to a constant (but small) value of $|\psi(z,t)|$ enclosing the path followed by a moving quasi-node. Within these tubes, $|\vec{\Omega}(z,t)|$ takes on large values, but the vorticity vanishes outside of these tubes (because $\psi(z,t)$ is an analytic function in these regions).

The remainder of this study is organized as follows. Computation of quantum trajectories is described in section 2, and eight types of reflected and transmitted trajectories are described in section 3. A series of time slices showing trajectory locations are presented in section 4, and vertical tubes and two types of reflected trajectories are described in more detail in section 5. Finally, a summary appears in section 6.

2. Propagation of Quantum Trajectories

Before presenting the method used to propagate quantum trajectories, the scattering problem will be briefly described.[1,2] The initial wave packet in z-space is given by

$$\psi(z) = (2\beta/\pi)^{1/4} e^{-\beta(z-z_0)^2} e^{ik_0(z-z_0)} \tag{1}$$

where the translational energy is $E = \hbar^2 k_0^2/(2m)$. This function is centered at the position $z_0 = (x_0,0) = (6,0)$, the width parameter is $\beta = 6$, and the mass is $m = 2000$ (all parameters are given in atomic units). The complex-valued Gaussian potential is given by

$$V_G(z) = V_0 e^{-\gamma(z-z_b)^2} \tag{2}$$

This barrier is centered at $z_b = (x_b,0) = (9,0)$, the width parameter is $\gamma = 4$, and the barrier height on the real-axis is $V_0 = 0.035$. The initial wave packet energy is $E = V_0/4$.

Quantum trajectories in the complex plane are obtained by integrating the equation of motion

$$\frac{dz(t)}{dt} = \frac{p(z,t)}{m} \tag{3}$$

where the quantum momentum function is obtained from the wave function through the relation

$$p(z,t) = \frac{\hbar}{i}\frac{1}{\psi(z,t)}\frac{\partial\psi(z,t)}{\partial z} \tag{4}$$

The real and imaginary components of the momentum vector, $\vec{p}(z,t) = [p_r(z,t),p_i(z,t)]$, are responsible for 'horizontal' and 'vertical' components of motion in the complex plane. This function possesses two special points of interest: poles occur at *nodes* where $\psi(z,t) = 0$, and $p(z,t)$ becomes zero at *stagnation points* where $d\psi(z,t)/dz = 0$ (and $\psi(z,t) \neq 0$). In addition, as described in detail in our earlier studies, the quantum momentum field exhibits *hyperbolic flow* around quasi-nodes in the density (these are local minima where the amplitude becomes small but does not reach zero). In order to analyze this flow, the Pólya vector field was introduced, and maps of this field show circular counterclockwise flow around quasi-nodes and hyperbolic flow around stagnation points.

The following procedure was used to propagate trajectories across the computational grid. At each time step, it is necessary to find the indices of the corner grid points for the cell in the computational grid in which the trajectory is located. These indices for the four grid points at the corners of this cell are denoted (j_0,k_0), (j_0+1,k_0), (j_0,k_0+1), and (j_0+1,k_0+1). Since the wave function is known at each of these points, $d\psi/dz$ may be computed at each corner point using wave function values known at neighboring grid points. Equation 4 was then used to compute the quantum momentum function at each corner grid point. Finally, linear interpolation was used to find the quantum momentum at the position of the trajectory within this cell. This procedure was then repeated for each trajectory at each time step.

3. Types of Quantum Trajectories

Starting from a Cartesian grid near the center of the initial wave packet, hundreds of quantum trajectories were launched toward the barrier region. Although it is trivial to categorize these trajectories as either 'transmitted' or 'reflected', it is more subjective to group the reflected trajectories into the seven categories listed in Table 1. It is useful to note that some of the reflected trajectories display simple behavior, while others display very complicated motions. Some propagate directly toward the barrier region, while others tend to move either up or down relative to the vertical (imaginary) axis. The complicated reflected trajectories arise because of quantum vortices that develop above the real-axis. Some of the quantum trajectories become trapped near transient stagnation points located between the vortices, while others execute complex loops or spirals as they escape from or avoid these regions.

Figure 1 shows plots for four of the eight trajectory categories listed in Table 1. The vertical coordinate is the propagation time, and these trajectories were propagated for 1000 atomic time units. In each figure, isosurfaces having constant values of the potential energy are shown. Of course, the potential is independent of time, so that each isosurface appears as a curved vertical slab. The real-axis, when displaced vertically in time, is outlined by the red box. Part (a) of this figure shows six *transmitted trajectories*, of which two barely make it to the transmitted side of the barrier. In part (b), seven *spiral trajectories* are shown. These trajectories initially move to larger values of y, but after about $t = 600$, they spiral back toward the real axis. In part (c), 22

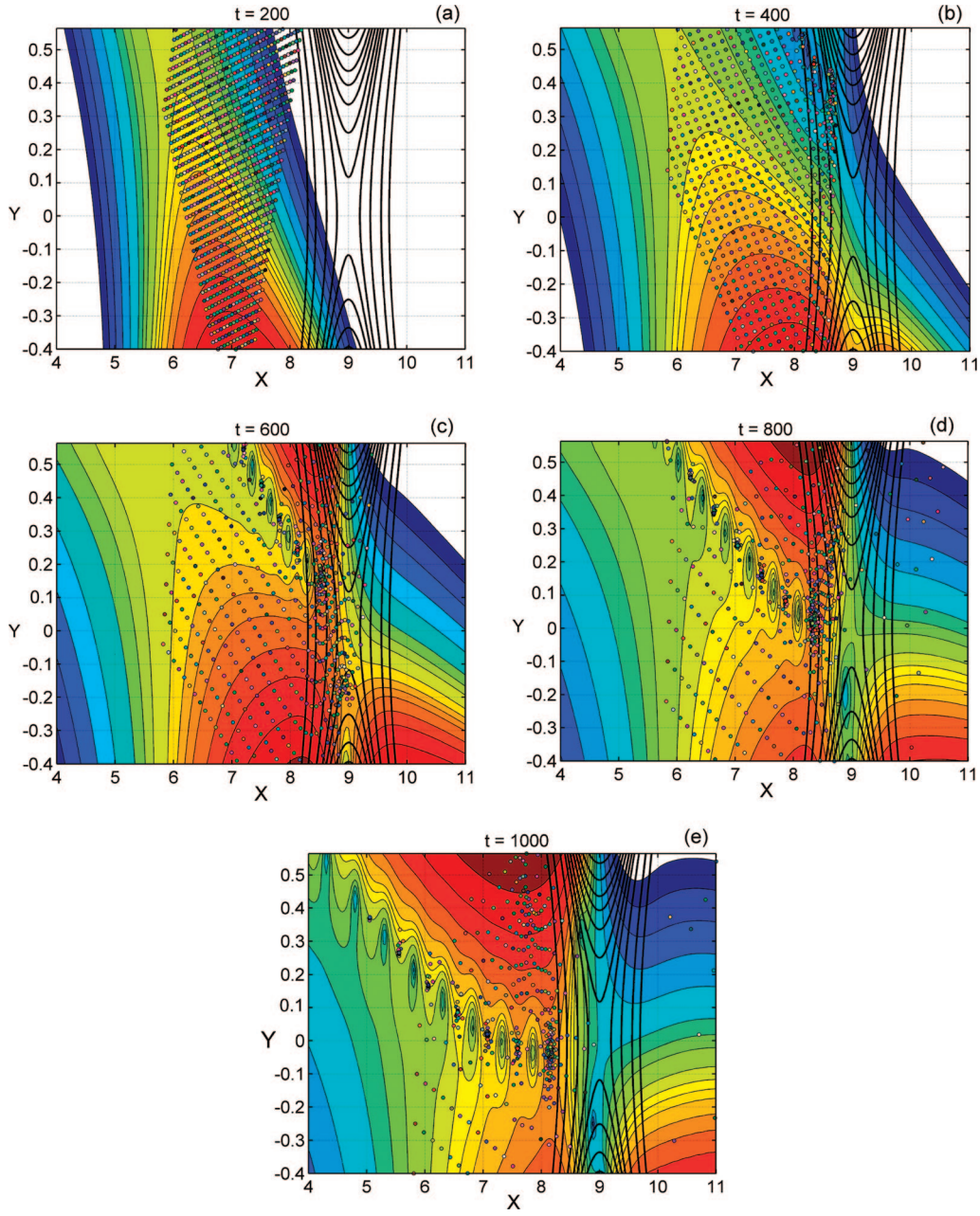

Figure 3. Contours (color) of $\log_{10}|\psi|$ showing propagation of the wave packet in the complex plane. Contours (black) of the magnitude of the potential, $|V(z)|$, are shown on the right side of the figure. In addition, locations the quantum trajectories are shown (colored dots).

twist trajectories are plotted. After reflection from the barrier, these trajectories execute at least one twist as they move toward smaller values of y. Finally, in part (d), 5 *loop-simple trajectories* are shown. As these trajectories approach the barrier region, they move upward toward more positive values of y, and then reflect down toward smaller y values, without looping or spiraling. In the next section, we will observe that twist and spiral trajectories acquire their complicated motions by passing close to quasi-nodes, where they are strongly influenced by the repulsive quantum potential. Of the seven types of reflected trajectory listed in Table 1, only the *loop-simple* and *upper* trajectories are *not* strongly influenced by the quasi-nodes that form on the reflected side of the barrier. Trajectory dynamics near the vortical regions are described in more detail in section 5.

4. Quantum Trajectory Dynamics

Quantum trajectory evolution was studied by launching a set of trajectories from a rectangular grid located near the starting position of the initial wave packet. In Figure 2, the colored dots show the initial positions of 1935 trajectories superimposed upon a color-fill contour map of the amplitude of the initial wave function. Note that the amplitude has significantly higher values below the real-axis. The trajectories were propagated for the time $t = 1000$, and during this interval some trajectories transmitted to the right side

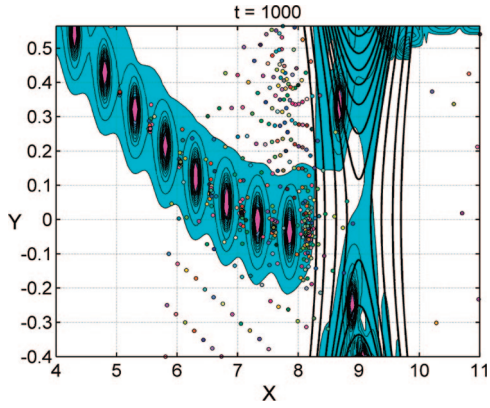

Figure 4. Absolute value of the quantum potential at time $t = 1000$. The pink regions between $x = 4$ and $x = 8$ locate eight quasi-nodes that gradually move toward the lower left. The quantum trajectories (colored dots) are repelled from regions of high quantum potential. Clusters of trajectories are noted around transient stagnation points near the quasi-nodes.

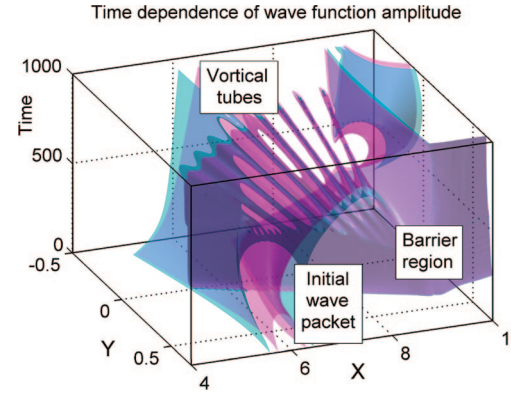

Figure 5. Two isosurfaces of $\log_{10}|\psi(z,t)|$ are drawn for the values °0.6 (inner pink surface) and °0.9 (outer cyan surface). The initial wave packet is centered near $z_0 = (6,0)$, and the barrier is centered near $z_b = (9,0)$. Starting around $t = 350$, several vorticity tubes develop in the region above the real-axis. As time proceeds, these tubes bend back toward the real axis.

of the barrier, but most moved back to the left during the formation of the reflected wave packet.

Snapshots of the quantum trajectories and the amplitude of the wave function are shown at five time steps in Figure 3. Each trajectory always carries the same color, so it is possible to follow some of the trajectories as they interact with the potential. In part (a), the trajectory grid undergoes a shearing deformation when trajectories on the front edge of the wave packet are thrust upward with high speeds, while those on the upper left move down toward the real-axis with low speeds. In part (b), trajectories on the upper right are starting to form clusters when the wave packet begins to reflect from the upper part of the barrier potential. In part (c), a series of five quasi-nodes is forming above the real-axis from about $x = 6.5$ to $x = 8.5$. Some of the quantum trajectories are clustering near stagnation points located to the lower-right or upper-left of each quasi-node. Also, a few trajectories have crossed over to the transmitted side of the barrier. In parts (d) and (e), these quasi-nodes move further toward the lower-left of the figure as the reflected wave packet recedes from the barrier region. Some of the quasi-nodes in part (e) are moving across the real-axis, where an observer would detect 'interference oscillations' in the amplitude and density.

We will see in section 5 that trajectories trapped near stagnation points (which themselves are time-dependent) move away from the barrier region in correlated groups. In addition, trajectories become 'indented' when they temporarily follow hyperbolic paths near quasi-nodes. The quasi-nodes modify the local trajectory dynamics through the intense quantum potential and the resulting strong quantum forces in there regions. The absolute value of the quantum potential at time $t = 1000$ is shown in Figure 4. The pink regions of high quantum potential between $x = 4$ and $x = 8$ locate eight quasi-nodes that continue to move toward the lower left. The quantum trajectories (colored dots) are repelled from regions of high quantum potential. Clusters

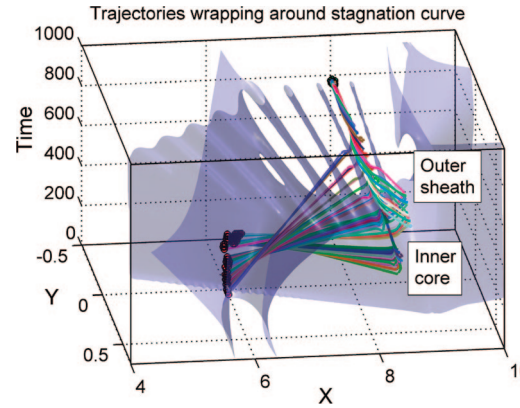

Figure 6. Quantum trajectories (colored lines) wrapping around the stagnation curve between vorticity tubes 1 and 2. One isosurface of $\log_{10}|\psi(z,t)|$ is drawn for the value °0.7. Trajectories launched from positions relatively far from the real-axis form the tight inner core of the bundle, while trajectories launched closer to the real-axis form the loosely bound outer sheath.

of trajectories are noted around pairs of transient stagnation points which form close to each quasi-node (especially near $x = 8$).

5. Trajectory Dynamics near Vorticity Tubes

Trajectory dynamics within the reflected wave packet is strongly influenced by multiple quasi-nodes that form above the real-axis and which subsequently move toward the region below this axis as the reflected packet recedes from the barrier region. In order to explore features of quantum trajectories near these quasi-nodes, the trajectories will be plotted on the type of three-dimensional diagram shown in Figure 5, where propagation time appears on the vertical axis above the complex plane. (In Figures 5−8, note that the positive y-axis is pointing *toward* the viewer.) In this figure, isosurfaces have been plotted for two constant values of the wave function amplitude. As the initial wave packet scatters

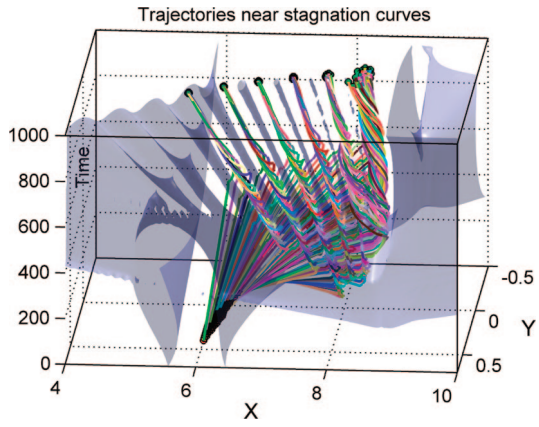

Figure 7. Quantum trajectories wrapping counterclockwise abound six stagnation curves which form near the vorticity tubes (487 trajectories are plotted). As we progress from stagnation curve 1 on the right to curve 6 on the left, the trajectories become more tightly wrapped. One isosurface of $\log_{10}|\psi(z,t)|$ is drawn for the value °0.7.

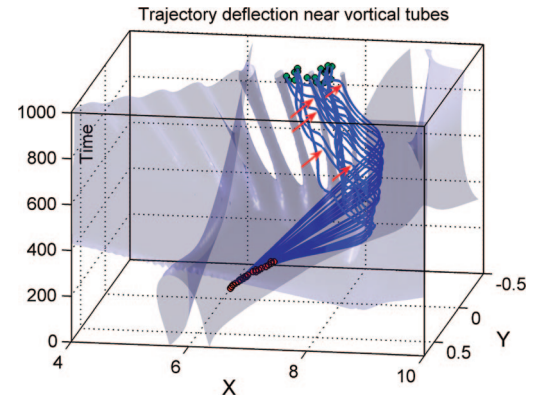

Figure 8. Trajectories deflecting around two vorticity tubes (22 trajectories were plotted). When each trajectory passes close to a tube number 1 or number 2, it follows a hyperbolic path. The five red arrows show hyperbolic indentations as the trajectory passes near a tube.

from the barrier region on the left side of the figure, a vorticity tube surrounds each of the quasi-nodes that forms above the real-axis. Each tube encloses a region of low amplitude, one of the quasi-nodes. As time proceeds, the reflected wave packet moves away from the barrier region, which causes these tubes to bend toward (and extend below) the real-axis.

In order to elucidate the dynamics, a large number of quantum trajectories (1521) were launched from a 39 × 39 grid located near the center of the initial wave packet. This grid covered the range [0.4,−0.55] along the y-axis and [6,6.95] along the x-axis. (This grid is slightly different from the one shown earlier in Figure 5.) All of these trajectories were plotted, but only those that eventually propagated near the vorticity tubes will be described in this section. In Figures 5− 8, sets of quantum trajectories are plotted, along with one or more isosurfaces of the wave function amplitude.

In Figure 6, 57 quantum trajectories (colored lines) are shown wrapping counterclockwise (when viewed from the -y direction) around the stagnation curve that forms between vortical tubes 1 and 2. (These tubes are numbered consecutively from the barrier region out toward the location of the initial wave packet.) There are three types of trajectories that eventually wrap around this stagnation curve. Trajectories launched from positions relatively far from the real-axis (between $y = -0.45$ and -0.55) gather in the time interval $t = 300-350$ to form the tight inner core of the bundle. After that, trajectories launched slightly closer to the real axis (between $y = -0.40$ and 0.48) gather in the time interval $t = 450-750$ to form the middle segment of the bundle. Finally, trajectories launched closer to the real-axis (between $y = 0.05$ and 0.35) gather in the time interval $t = 550-750$ to form the more loosely bound outer sheath. Even though trajectories from these three sets travel different distances with different velocities, they eventually become correlated and twist in unison around the stagnation curve.

In Figure 7, 487 quantum trajectories are shown wrapping counterclockwise abound six stagnation curves which form near vorticity tubes 1−7. As we progress from right to left, the trajectories become more tightly wrapped around the stagnation curves. The trajectories that wrap around a particular stagnation curve are launched from a specific curve in the $x-y$ plane. Finally, in Figure 8, 22 trajectories are shown deflecting around vorticity tubes 1 and 2. When each trajectory passes near one of these tubes, it is first drawn in toward the tube before repelling away (along a hyperbolic path). The red arrows show indentations in five trajectories as they pass near these tubes.

6. Summary

In this study, exact quantum trajectories were analyzed for the barrier scattering problem that was computationally investigated in our previous papers.[1,2] These exact quantum trajectories were computed by integrating equations-of-motion involving $p(z,t)$, the quantum momentum function, which in turn was obtained from the time-dependent wave function. Thousands of quantum trajectories were launched from positions near the center of the initial wave packet, and trajectory evolution was illustrated in space-time diagrams. These trajectories were divided into several categories, depending upon whether they were transmitted or reflected during the scattering process and upon the complexity of the dynamics in the reflected region. Special emphasis was placed upon selected sets of reflected trajectories. Among the most interesting are those that follow counterclockwise helical paths as they wind, like cooked spaghetti, around stagnation curves that form adjacent to quasi-nodes (where the amplitude reaches a local minimum) in the reflected wave packet. The trajectories that wrap around the stagnation curves originate from different regions near the center of the initial wave packet. In addition, other reflected trajectories follow hyperbolic paths when propagating near vorticity tubes which surround these quasi-nodes. As the reflected wave packet recedes from the barrier region, these tubes move away from the barrier region and eventually cross the real-axis, where an observer would detect ‘interference oscillations’ in the density. However, this observer would

be clueless regarding the rich dynamics ensuing in the complex space that preceded these observations.

Acknowledgment. This research was supported in part by funding from the Robert Welch Foundation. We thank Julianne David and Chia-Chun Chou for helpful comments.

References

(1) Wyatt, R. E.; Rowland, B. A. To be published.

(2) Rowland, B. A.; Wyatt, R. E. To be published.

(3) Chou, C. C.; Wyatt, R. E. *Phys. Rev. A* **2006**, *76*, 012115.

(4) Chou, R. E.; Wyatt, R. E. *J. Chem. Phys.* **2008**, *129*, 124113.

(5) Sanz, A. S.; Miret-Artés, S. *Chem. Phys. Lett.* **2008**, *458*, 239.

(6) Chou, C. C.; Wyatt, R. E. *J. Chem. Phys.* **2008**, *128*, 234106.

(7) Pólya, G.; Latta, G. *Complex Variables*; Wiley: New York, 1974.

(8) Needham, T. *Visual Complex Analysis*; Oxford University Press: Oxford, 1997.

(9) von Helmholtz, H. J. *Für Reine Angew. Mathematik* **1858**, *55*, 25.

CT8002496